SEAMLESS HYPERSPECTRAL HIGH SPATIAL MOSAIC DERIVED FROM CHANG'E-1 IIM. Y. Z. Wu, Z. C. Wang, X. Tang, X. M. Zhang, Y. Chen, W. Cai. School of Geographic and Oceanographic Sciences, Nanjing University, Nanjing, 210023, China (wu@nju.edu.cn).

Introduction: The Chang' E-1 Interference Imaging Spectrometer (IIM) is a sagnac-based spatially modulated Fourier transform imaging spectrometer, which mapped the lunar surface with a spatial resolution of 200 m. Within the nominal wavelength range (480-960 nm), IIM has 32 continuous channels with a theoretical spectral resolution of 325.5 cm^{-1}. Most areas are repeatedly covered by two or three orbits with different geometries. IIM, the spatially modulated instrument, has no mobile apparatus together with good thermal protection its response is very stable by careful checking for radiance with multiple observations of the same location at various geometries.

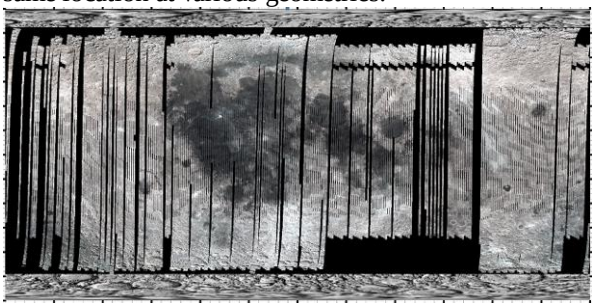

Fig. 1. IIM hyperspectral high spatial resolution mosaic (R-918 nm; G-776 nm; B-618 nm) using the method described in [1] with 151.6 px/d.

We finished the hyperspectral and high spatial resolution mosaic (Fig. 1) for IIM reflectance data (radiance factor, RADF) at standard geometry (30°, 0 °, 30 °) which were processed using the pipeline described in [1]. The bad point, stripe and inhomogeneity of sensor response were removed (Fig. 2). The boundaries of the mosaic between adjacent orbits are invisible (e.g., Fig. 3). This seamless product can have several uses such as minerals [2, 3], elements and geology [4, 5], comparison of lunar irradiance model and absolute reflectance [6-12], calibration for Earth observation sensors [13-15] and separation of basaltic units. The accurate separation of basaltic units is very crucial to date ages and interpret surface geology. This work, however, is often difficult due to the lack of perfectly calibrated data because of obvious hue variation between orbital boundaries in the mosaic which obscures the separation of different geologic units. The seamless IIM mosaic together with other lunar mosaics such as SELENE [6], M^3 [7], colorful LRO-WAC and low-Sun WAC[10], Radar [16] and Diviner [17] will contribute to the lunar geologic mapping project.

The standard IIM reflectance products have been published [1] and we should provide users all the data including both mosaic and individual orbits. For individual orbits they can be used to compare the absolute reflectance of the same location with multiple observations (e.g., Fig.4). Users are welcome to contact us for these products. The mosaic is 26 bands (522-918 nm) because the first 5 bands and the last band were removed due to the low SNR. The size is 122 Gb for the mosaic and 120 Gb for all the individual orbits.

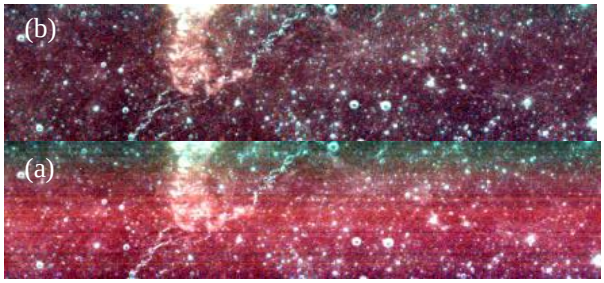

Fig. 2. Composite images of 918 nm (R), 757 nm (G) and 658 nm (B) of the raw IIM data (a) and the final calibrated data (b). North is to the left.

Product description: The lab spectral calibration was done with gas laser and semiconductor laser with spectral position accuracy of 0.04 nm @543 nm to 2.48 nm@831 nm. The full FOV radiometric calibration with average uncertainty of 3.56% was performed using an integration sphere and ASD traceable to NIST standard. The IIM signal chain is linear over most of the range (<1%) with a small nonlinearity at the lowest signal levels (2.5%) measured with an adjustable integrating sphere. Unfortunately, overexposure largely occurred at low latitude and many data are saturated. The IIM RADF was calculated using the solar irradiance spectra [18], which was the only one measured outside the Earth' atmosphere during low solar activity and also recommended by M^3 team [19].

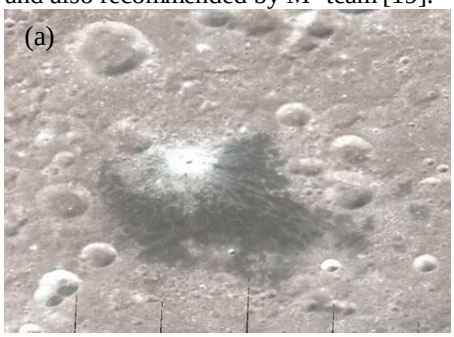

To build the reflectance model, the Moon was calssified into 4 classess (very bright rays, mature high-

lands, low-Fe basalts, and high-Fe basalts), perhaps the most classes of the existing models. The reflectance normalization was applied to each pixel by applying suitable model pixel-by-pixel. Although the pixel-level model increases noise, as shown in the mosaic (Fig. 3) the hue is homogeneous and no abrupt change, which demonstrates the quality of the photometric model.

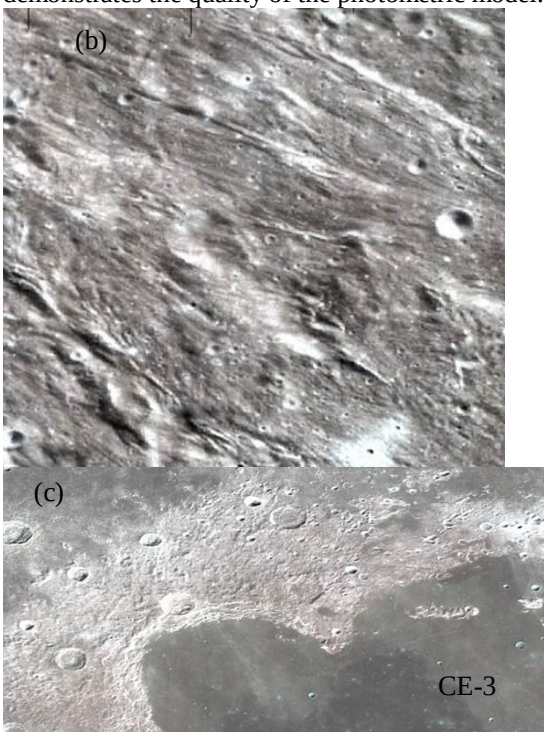

Fig. 3. Examples of hyperspectral mosaics of IIM reflectance data for north hemisphere (a), south hemisphere (b) and northwest Imbrium (c).

The IIM reflectance of the same location with multiple observations were validated by largely randomly selecting places spanning various geologic units and latitude. As examples Fig. 4 shows some representative calibration sites (Ap16W, MS2 and CE-3 area). The comparisons show that the IIM reflectance of the same location with multiple observations match very well with std less than 0.01, which also demonstrates the quality of our lunar model. All the orbital reflectance is much smaller than the Apollo sample (62231) reflectance. LRO WAC reflectance is the largest and most red among all the orbital reflectance. The absolute reflectance of IIM is much larger than the OP1B M^3 reflectance and comparable to OP2C1 M^3 reflectance. Note that the M^3 photometric model was derived from highlands and OP2C1 observations. In addition to the difference of lab calibration of instruments, the difference of the standard reflectance of these instruments is also related to the photometric model used. For example, the phase function ratio f(30°)/f(a) varies with surface albedo. For the reflectance normalization the phase function used should be consistent with their albedo. The IIM photometric model for CE-3 is the only one derived from the darkest basalts (Class 4).

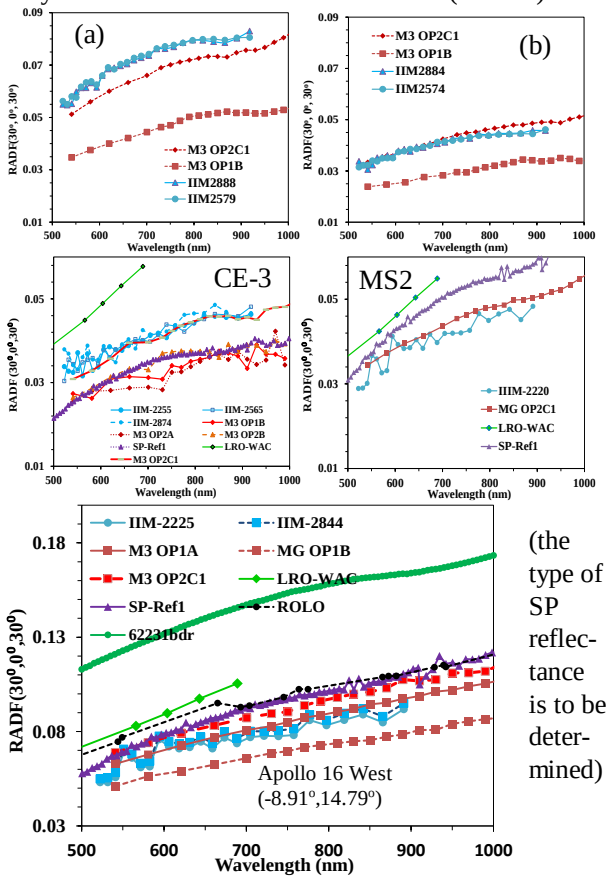

(the type of SP reflectance is to be determined)

Fig. 4. The IIM reflectance comparison of the same location with multiple observations and other data. (a) The brightest area in Sinus Iridum. (b) The darkest area in Sinus Iridum. Other areas are shown in the legend.

References: [1] Wu, Y. Z. et al. (2013) *Icarus*, 222, 283-295. [2] Wu, Y. Z. et al. (2010) *Planet Space Sci.*, 58, 1922-1931. [3] Wu, Y. Z. et al. (2010) *Sci. China Ser.*, 53, 2160-2171. [4] Wu, Y. Z. et al. (2012) *JGR*, 117, 1-23. [5] Wu, Y. Z. (2012) *Geochim. Cosmochim. Acta*, 93, 214-234. [6] Yokota, Y. et al. (2011) *Icarus*, 215, 639-660. [7] Besse, S. et al. (2013) *Icarus*, 222, 229-242. [8] Sato, H. et al. (2014) *JGR*, 119, 1775-1805. [9] Ohtake, M. et al. (2010) *Space Sci. Rev.*, 154, 57-77. [10] Wagner, R. V. et al. (2015) *LPS XLVI*, abstract #1473. [11] Velikodsky, Y. I. et al. (2011) *Icarus*, 214, 30-45. [12] Kieffer, H. H. (2005) *Astron. J.*, 129, 2887-2901. [13] Stone, T. C. et al. (2005) *Optics Photonics*, 5882, 58820. [14] Kouyama, T. et al. (2014) *LPS XLV*, abstract #1302. [15] Miller S. D. et al. (2009) *IEEE 4*, 2316-2329. [16] Morgan, G. A. et al. (2015) *LPS XLVI*, abstract #2180. [17] Paige, D. A. et al. (2010) *Space Sci. Rev.*, 150, 125-160. [18] Thuillier, G. et al. (2003) *Geophys. Monogr.*, 141, 171-194. [19] Green, R. O. et al. (2011) *JGR*, 116, E00G19.